TEL AVIV UNIVERSITY

Spin Dependent Transport

Alon Shaaltiel, Oren Kereth and Simon Salleh Atri

January 31, 2022

Abstract

By subjecting nickel, a ferromagnetic metal, to an external magnetic field in different orientations three effects were observed: the anomalous Hall effect, anisotropic magnetoresistance and the planar Hall effect. Using the measurements, characteristics of the crystalline structure of nickel were studied and also its magnetic properties were compared to values from the literature.

Part I
Theory

1 Magnetization

When an external magnetic field H, is applied to a material, the response of the material is called magnetic induction, B. The equation relating the two is

$$B = H + 4\pi M \tag{1}$$

where M is the magnetization of the medium and is a property of the material. M depends on moments of the atoms, ions and molecules and their interactions as will be later explained. The ratio of M to H is also a property of the material as it indicates the way the material responds to an external magnetic field

$$\chi = \frac{M}{H} \tag{2}$$

where χ is called the susceptibility of the material. A similar ratio of B to H can also be calculated

$$\mu = \frac{B}{H} \tag{3}$$

where μ is called the permeability of the material and indicates how permeable the material is to a magnetic field. Some materials have negative susceptibilities, for example, diamagnets, upon exertion of an external field, they reject the field by creating a magnetization in the opposite direction. Some materials have a constant susceptibility (i.e. a linear relation between H, M) such as paramagnets. Others have non-zero magentization with no external field and their susceptibility changes for different values of H . Ferromagnets follow that criteria and by plotting their corresponding $M-H$ and $B-H$ curves a *hysteresis loop* can be seen (see Figure 1).

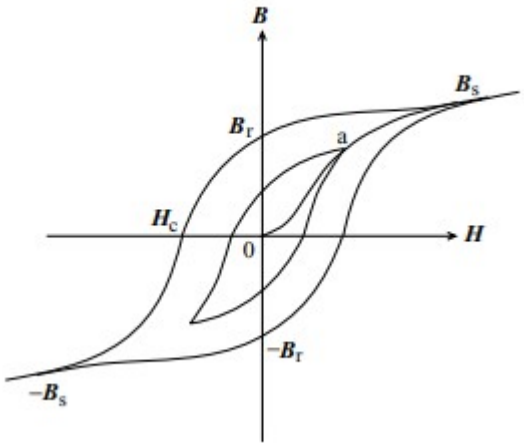

Figure 1: Hysteresis loop of a ferromagnet [8]

Note that the changes in M and in B are non-linear in H. Moreover, the $M-H$ curve is in this case a loop, , meaning that for the same value of H two values of M

are to be expected, depending on the way the loop is traced. The magnetization also reaches 'saturation' for a sufficiently large external field as can be seen in the edges of the loop. This saturation indicates that all the dipoles in the material have turned and are parallel to the external magnetic field, yielding maximal magnetization. After reaching saturation, the hysteresis loop shows that a non-zero external field is required to reach $B = 0$, that non-zero field, H_c, is called the coercivity of the material. Magnets that require a large field to do so are called 'hard' while magnets that are easily saturated and demagnetized are called 'soft'.

2 Origin of Magnetization

2.1 Magnetic Moment of Electrons

After analysing the macroscopic properties of ferromagnets and other materials, let us review the microscopic origins of the magnetization. Materials consist of atoms that are made of electrons, protons and neutrons. The electrons are bound to the nucleus via the Coulumb interaction. Solving the Schrödinger equation for the bound states in a hydrogen atom, which consists of one electron and one proton, yields the exact solutions

$$|\psi >= |nlm_l > \tag{4}$$

where n ,l and m_l are three quantum numbers that restrict the energy of the bound electron, its orbital angular momentum and the orientation of its orbital angular momentum with respect to some magnetic field respectively. Orbitals of the electrons are named s,p,d,f and so on, corresponding to an orbital angular momentum of $l = 0,1,2,3$ respectively. Because electrons are charged particles that carry angular momentum they also have a magnetic moment, therefore they generate magnetic fields and interact with magnetic fields. The magnetic moment of the electron consists of two terms, one from its orbital angular momentum and one from its 'internal' angular momentum- its spin. There are two qunatum numbers relating to spin. The first is spin quantum number, s, which always equals $\frac{1}{2}$ and is analogous to the quantum number l. The second is m_s which is the spin analog to m_l and in this case is only allowed to take the values of $\frac{1}{2}, -\frac{1}{2}$. Thus, the magnetic moment of an electron is

$$\boldsymbol{m} = -g_e\mu_B m_s - \mu_B m_l \tag{5}$$

where μ_B is the Bohr magneton and is defined as $\mu_B = \frac{e\hbar}{2m_e}$ where e, m_e are the electron's charge and mass respectively and $\hbar$ is the reduced Planck constant. g_e is called the g-factor of an electron and is approximately 2. The total magnetic moment of the material, made up of small electronic moments, forms the magnetization of the material when it interacts with a magnetic field.

2.2 Pauli's Exclusion Principle & Larger Atoms

Moving to atoms containing more electrons and more protons, it is essential to understand their energy states and how they differ from the case of an hydrogen atom. Using perturbation theory [5] one can find that electrons with lower angular momentum (i.e. lower values of l) are lower in energy. In order to fill the unoccupied energy states with electrons, Pauli's exclusion principle must come into account. Pauli's exclusion principle states that the total-electron wavefunction (the wavefunction describing all the electrons in the atom in this case) must be anti-symmetric with respect to any interchange of two electrons. It can be directly inferred that no two electrons can occupy the same state (i.e. having the exact same quantum numbers). As a result, only two electrons may occupy each atomic orbital, one with spin 'up' ($m_s = \frac{1}{2}$) and the other with spin 'down' ($m_s = -\frac{1}{2}$). In order to compute the total magnetic moment of the electrons in the atom, another effect must be taken into account- spin orbit coupling. In short, because the electron has an orbital momentum and there is an effective current, a magnetic field is formed. The spin of the electron then interacts with that magnetic field, altering the energy states and creating more favourable spin and angular momentum states for the electrons to occupy compared to others.

3 Ferromagnets

In this section different effects contributing to ferromagnets are explained.

3.1 Exchange Energy

When there is more than one electron surrounding the nucleus the Coulumb interactions between them should be accounted for. There are two different wave-function configurations that are possible- one which is spatially symmetrical under the exchange of two electrons but its spinor is anti symmetrical and vise-versa. Using perturbation theory to take into account the effect of the interactions between electrons, in the case of two electrons the energy states are

$$E = E_1 + E_2 + K \pm J \tag{6}$$

where E_1, E_2 are the energies of the two electrons without the perturbation, K is a perturbation term which is not dependent on the wave-function's configuration (i.e. the spinor's symmetry), and the last term, J, is called the exchange energy, its contribution to the energy is dependent on the configuration of the wave-function . + is for the configuration of two anti-parallel spins (anti-symmetrical spinor) and − is for the configuration of two parallel spins (symmetrical spinor). The implication of this result is that one spin configuration is more favourable compared to the other. In the case of $J > 0$ the electrons will prefer to align their spins as it is more energetically favourable, yielding spontaneous magnetization without any external field. However, there are more effects taking place that need to be taken into account.

3.2 Collective Electron Theory of Ferromagnetism

The alignment of electrons in the same direction is opposed by the band energy involved in transferring electrons from the lower energy states that are entirely occupied to the higher energy states that are partially occupied. In ferromagnets, the Fermi energy lies in a region of overlapping 3d and 4s states. Due to the high density of states near the Fermi level in the 3d orbital and the low density in the 4s orbital, the 3d states are effected by exchange interactions while 4s states are not. Therefore there is a preferred spin alignment . Because there is exchange splitting in that region and the 3d orbital is only partially occupied, there will be spontaneous magnetic moment (and therefore it is a ferromagnet). If the Fermi energy lies above the 3d orbital, despite the exchange interaction taking place in the 3d orbital, all 3d states will be filled with down and up spin electrons, thus negating the magnetic moment. The difference in the Fermi energy can make the difference between a ferromagnet and a simple metal.

3.3 Domains

Despite the exchange interaction that suggests that ferromagnets should be magnetized with all of the electrons having the same parallel spin, they are not. Instead, ferromagnetic domains are formed, where all the spins are aligned parallel to each other . The average magnetization is therefore 0. The domains are formed in order to minimize other contributions to the total magnetic energy.

3.3.1 Magnetostatic Energy

If all the spins in the material were parallel to each other, a large magnetic field would have formed, with a corresponding energy of

$$U_H = \frac{1}{4\pi} H_d^2 \tag{7}$$

where H_d is called the demagnitizing field and is essentially the field created by the magnetized ferromagnet. U_H is the energy stored in that demagnetizing field (maybe refernce griffith or something idk). By forming more domains with different spin alignments, the demagnetizing field is reduced, thus minimizing the magnetostatic energy while maximizing the exchange energy in each domain (see Figure 2).

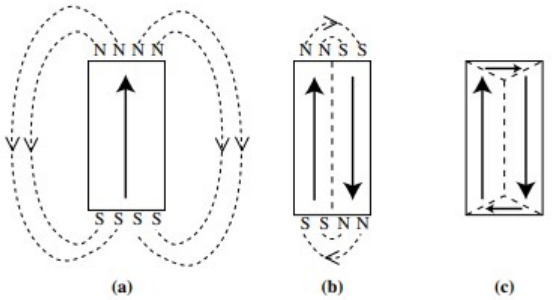

Figure 2: Reduction of the magnetostatic energy by domain formation [8]

The shape of the domains and their orientation is also dependant on the magnetocrystalline energy and magnetostrictive energy.

3.3.2 Magnetocrystalline Energy

The magnetization in ferromagnetic crystals tends to align along certain preferred crystallographic directions. The preferred directions are called the "easy" axes, since it is easiest to magnetize a demagnetized sample to saturation if the external field is applied along a preferred direction [8] and the "hard" axes are those that require the most energy in order to magnetize (i.e. larger external field to reach saturation). The energy difference per unit volume between samples magnetized along easy and hard axis is called the magnetocrystalline anisotropy energy. In order to minimize the magnetocrystalline energy, the domains will form such that their spins point along easy axis. Within the interface between domains the direction of magnetization changes, and therefore cannot be aligned along an easy axis, thus increasing the energy. Therefore, the magnetocrystalline energy favors a few domains with less boundaries over many domains with many boundaries .

3.3.3 Magnetostrictive Energy

When a ferromagnetic material is magnetized it undergoes a change in length known as magnetostriction. Domains with different orientations that are near each other cannot elongate at the same time, for example, in figure 2 the vertical and horizontal domains are unable to elongate simultaneously along their corresponding spin directions. As a result, an elastic strain energy term is added to the total energy. This energy favors small closure domains and therefore favors many small domains. The domains are thus formed as an optimization of the energies above.

4 Ferromagnetic Effects

Due to the nature of ferromagnets, some unusual effects regarding the resistance of the ferromagnet can be measured. This experiment will revolve around these important effects.

4.1 Hall Effect

Suppose there is a block of metal (see Figure 3) , by applying an electric field in the x direction (using a battery with some known voltage V_x) an electric current I with a corresponding current density J_x starts flowing through the metal in the same direction.

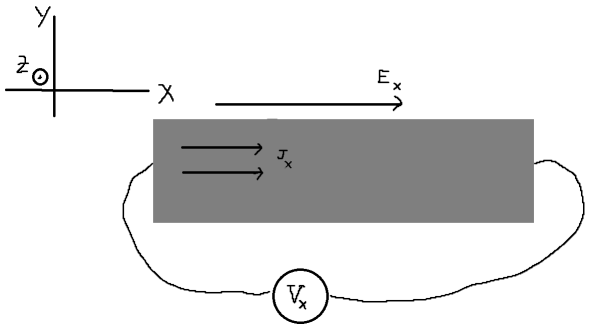

Figure 3: Ohm's Law. An electric field E_x generates current density J_x in a block of metal

This is Ohm's law which can also be derived from Drude's equation [7]. Now, suppose a magnetic field, H, is applied in the z direction in addition to the existing electric field. The magnetic field will interact with the flowing electrons through Lorentz force and deflect the electrons to the y direction. As a result, negatively charged electrons will accumulate on one side of the metal block while the other side will become positively charged due to the vacant electrons. These charges will

then generate an electric field in the y direction, E_y, and in a steady state a voltage can be measured in that direction (see Figure 4).

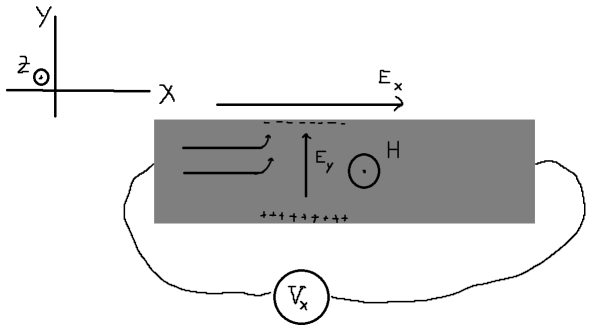

Figure 4: Hall Effect. The magnetic field creates a measurable voltage in the y direction.

The electric field in the y direction and the current density J_x are related through the Hall coefficient

$$E_y = R_H H J_x \tag{8}$$

where R_H is the Hall coefficient and is defined as

$$R_H = -\frac{1}{ne} \tag{9}$$

where e is the charge of the electron and n is the charge density. It is important to note that this effect is negative for positive magnetic fields, meaning that if $R_{xy} \equiv \frac{V_y}{I_x}$ is measured and is plotted against the magnetic field H, a linear curve with a negative slope is to be expected. This linear curve is anti-symmetrical for the exchange of $H \rightarrow -H$.

4.2 Anomalous Hall Effect

While The Hall effect can be measured in simple metals, the anomalous Hall effect (AHE) is unique to ferromagents. Suppose the metal block from the previous section is now a ferromagnetic plate and magnetized in a direction perpendicular to the plane of the plate. A current is passed through the plate in the x direction and the electrons in the current be scattered by the magnetized atoms. The scattering will turn out to be asymmetrical as explained later in this section. As a result a charge will build up on the edges of the plate, creating an electric field in the y axis according to

$$E_s = R_s M J_x \tag{10}$$

where E_s is the electric field in the y axis, M is the magnetization of the plate and R_s is referred to as the anomalous Hall coefficient. The anomalous Hall resistivity is far greater by magnitude than the normal Hall effect.

Let us explain the anomalous Hall effect using a microscopic analysis of the conductance band and its overlapping part with the 3d shell. As mentioned in a previous section, the 3d orbital is effected by the exchange interaction due to the dense energy states, thus a clear split between up and down spin electrons in this orbital occurs, with parallel spin electrons being a more energetically favourable configuration until the energy gaps force otherwise. The spin up electrons are shifted down while the spin down electrons are shifted up. In addition to the exchange interaction affecting the d-states, spin-orbit coupling creates further divisions as it removes the degeneracy of different m_l values for the spin up and down electrons (see Figure 5)

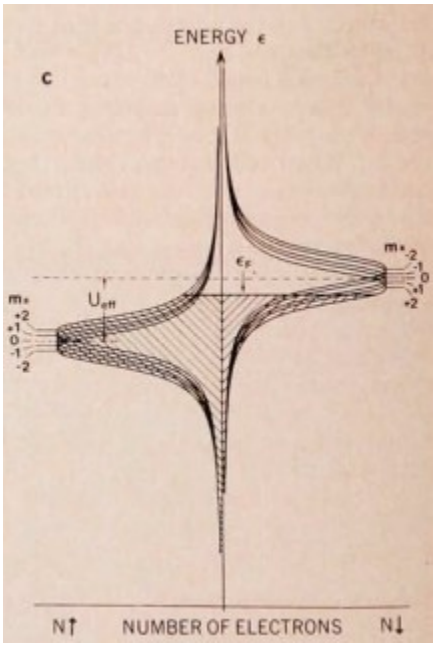

Figure 5: Density of states for the d-level of a ferromagnet [1]

In the case shown in the figure, with the Fermi energy being where it is, the spin up states are nearly filled whereas the spin down states are filled only for the $m = 2$ states, therefore the conduction electrons flowing through the metal have a far greater chance to be scattered into one of the $m = 2$ states than into the $m = -2$, creating an asymmetric scattering which gives rise to the anomalous Hall effect. If the Fermi level lies above the maximum of the spin-down resonance the density of $m = -2$ states exceeds that of $m = +2$ states, and the asymmetry in the scattering changes its sign. This is the case in Nickel, the metal we are working with in this experiment, and so the anomalous Hall resistance is negative for positive magnetization (parallel to the z axis) . In Nickel, combining the anomalous Hall effect with the normal Hall effect explained in the previous section, the total resistivity R_{xy} as defined previously, increases in magnitude for increasing external magnetic fields due to the two Hall coefficients sharing the same negative sign (whereas for iron, whose Fermi energy lies below the maximum of spin down resonance the two effects interfere with one another). This phenomenon will be shown later in this report. Due to the dependency of the AHE in the magnetization of the ferromagent, it reaches saturation once the magnetization reaches saturation, and an hysteresis loop is formed for the resistivity just as it is formed for the magnetization M. Therefore, by looking at the Hall resistivity curve information about the material and its magnetization properties can be extracted as will be seen in later sections of this report.

4.3 Anisotropic Magnetoresistance (AMR)

AMR is the change in resistance when a magnetic field is applied on a ferromagnetic metal or alloy, the change depends on the direction of the field relative to the current and is therefore anisotropic. Non-ferromagnetic metals also change their resistance under a magnetic field, this effect is called magnetoresistance (MR) and is much weaker. As the MR in a ferromagnetic metal is almost entirely from AMR, other sources of MR are not accounted for.

The origin of AMR is the spin–orbit coupling, the s electrons which are responsible for the conduction are scattered by the vacant part of the orbital angular momentum of the 3d electrons. As the magnetization direction rotates in response to the applied magnetic field, the 3d electron cloud deforms, and changes the amount of scattering of the conduction electrons. When the magnetization direction is perpendicular to the current direction, the scattering cross-section is reduced compared with the zero-field case, whereas when the magnetization direction is parallel to the current direc-

tion, the scattering cross-section is increased. This concept is illustrated in Figure 6.

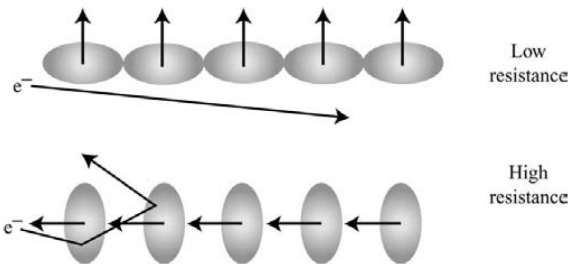

Figure 6: An illustrated representation of the AMR process [8].

The resulting effect on the measured magneto resistance is illustrated in Figure 7.

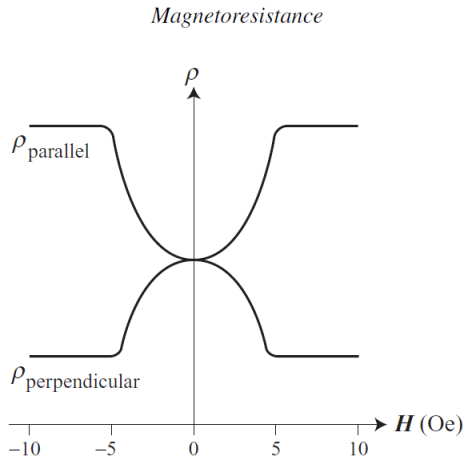

Figure 7: The changes to the magnetoresistance depending on the field's direction in reference to the current [8].

4.4 Planar Hall Effect (PHE)

Suppose there is a plate made out of a ferromagnetic material, an external magnetic field is exerted in the same plane as the plate and current is flowing through the plate in some direction $\hat{n}$. The angle between the magnetic field and $\hat{n}$ is θ, if $\theta = 0$ the effect detailed in the AMR section for a parallel field will occur and the resistance will be higher than without the field. If $\theta = \frac{\pi}{2}$ then the magnetic field will be perpendicular, lowering the resistance. For a general angle the resistance parallel to the current , denoted R_{xx} can be expressed as

$$R_{xx} = \rho_{par} cos^2\theta + \rho_{perp} sin^2\theta \tag{11}$$

where ρ_{par} is the resistance in the case of a parallel magnetic field (when $\theta = 0$ $R_{xx} = \rho_{par}$) and ρ_{perp} is the resistance in the case of a perpendicualr magnetic field (when $\theta = \frac{\pi}{2}$). For the resistance in the direction perpendicular to current flow, denoted by R_{xy}, there is a similar relation

$$R_{xy} = \frac{\rho_{perp} - \rho_{par}}{2} sin(2\theta) \tag{12}$$

These two expression can be found using the resistibility matrix and applying rotations on it. This matrix in the case of a parallel field ($\theta = 0$) is

$$\rho_0 = \begin{bmatrix} \rho_{par} & 0 \\ 0 & \rho_{perp} \end{bmatrix} \tag{13}$$

Where the diagonal elements are R_{xx} and R_{yy} for the two distinct cases of current flowing in $\hat{n}$ or perpendicular to it respectively. If the current is perpendicular to $\hat{n}$ it is also perpendicular to the magnetic field and thus $R_{xy} = \rho_{perp}$ in this case . In order to find the resistibility matrix for a general angle θ, this matrix should be rotated using a rotation matrix around the z direction. After rotating, the resistibility matrix turns out to be

$$\rho_{planar}(\theta) = R^{-1}\rho_0 R = \begin{bmatrix} \rho_{par} cos^2\theta + \rho_{perp} sin^2\theta & \frac{\rho_{par}-\rho_{per}}{2} sin(2\theta) \\ \frac{\rho_{par}-\rho_{per}}{2} sin(2\theta) & \rho_{perp} cos^2\theta + \rho_{par} sin^2\theta \end{bmatrix} \tag{14}$$

In this part of the experiment the resistibility matrix will be found by exerting a constant magnetic field and changing its angle compared to the sample.

Part II
Experimental Setup

As previously mentioned, in this experiment we will be using a nickel plate whose curie temperature is well above room temperature [2], and therefore will be in its ferromagentic phase in all the following measurements. This nickel plate has a known thickness of $10nm$ and is deposited on a crystal substrate which is mounted on a chip carrier (see Figure II).

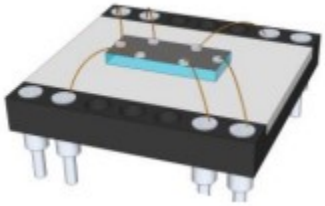

Figure 8: The experimental setup- schematic of the sample and the chip carrier

The chip carrier is connecting into a rotating base and inserted into an electromagnet. The chip carrier is connected to a multimeter that can perform a 4 probe measurement (see Figure 9)

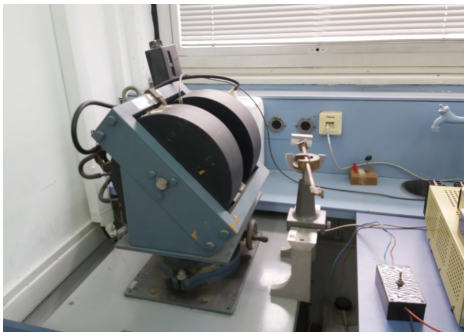

Figure 9: The experimental setup- electronmagnet and rotating base

Using a Lakeshore Model 425 Gaussmeter, the magnetic field applied by the electromagnet was be measured. The magnetic field is created using current flowing through coils, the current can be changed and its direction can be reversed using a button. Throughout this experiment, the resistance of the nickel sample in any given direction was be measured simultaneously with the magnetic field.

5 AHE

In this part of the experiment we are interested in R_{xy}. The magnetic field was changed and the resistance perpendicular to the direction of flow was measured. Using these measurements information regarding nickel's ferromagnetic properties was extracted, as will be further explained later in this report. By measuring both the anomalous and normal Hall effects and using the known values of R_s for nickel its saturation magnetization and charge carrier density were extracted as well. In order to create AHE the magnetic field was applied perpendicular to the current flow direction with magnitudes ranging between $-4300\,[Gauss]$ and $4300\,[Gauss]$.

6 PHE

In this part of the experiment, the magnetic field was applied in the same plane as the current's flow direction and θ , the angle between the current flow direction and the applied field was changed by rotating the base. For each angle the resistance both in the current flow direction and perpendicular to it was measured and the magnitude of the magnetic field remained constant throughout this experimental section. Using these measurements the resistivity matrix from equation 14 of the sample was extracted.

7 AMR

In this part of the experiment the resistance was measured parallel to the current's flow direction. The magnetic field was be applied in different directions and the change in resistance correlating to each direction and magnitude and magnetic field was measured. The expected results can be seen in Figure 7. The magnetic

field was applied perpendicular to the current, transverse to it and parallel to it. The change in saturation resistance (where the magnetization reaches saturation) between magnetic field direction was extracted using the measurements

$$\frac{\Delta\rho}{\rho} \equiv \frac{\rho_{per} - \rho_{par}}{\rho_{avg}} \tag{15}$$

where ρ_{per} is the saturation resistance when the magnetic field was perpendicular to the current, ρ_{par} when the magnetic field was parallel and ρ_{avg} is the average of all resistances with all magnetic field directions for the saturated nickel. Similarly to the previous part, information regarding the ferromagentic properties of nickel such as its easy axis and more was extracted using these measurements.

Part III

Measurements

8 AHE

By changing the magnetic field perpendicular to the sample and measuring the resistance perpendicular to the current flow, a hysteresis loop was traced due to the relation of AHE with the magnetization of the material. The saturation resistance (for which AHE saturates and the normal Hall effect starts to dominate) was found by fitting pairs of linear fits, one fit was made after saturation, where the change in resistance is linear due to the normal Hall effect. The other linear fit was made before saturation but using measurements close enough to the approximated region. The saturation resistance was then approximated as the average intersection point of the linear fits (see Figure 10)

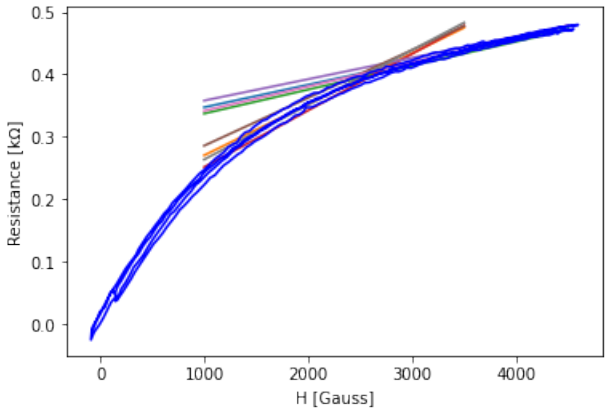

Figure 10: Linear fits at the saturation region

Using that saturation resistance and the known thickness of the sample, the saturation magnetization of the sample was found using the equation

$$\rho_H = \frac{R_0 H + 4\pi R_s M_s}{t} \tag{16}$$

where $t = 10nm$ is the thickness of the nickel sample, M_s is the magnetization of the nickel which we are interested in, ρ_H is the resistivity of the sample extracted from the measurements and R_0 is a constant resistance. The saturation magnetization came out to be

$$M_{saturation} = 4.01 \times 10^3 \pm 2.3 \times 10^2 (5.7\% R.E) \text{emu/cm}^3 \tag{17}$$

Furthermore, using the linear region where the normal Hall effect dominates, the normal Hall coefficient was extracted, from which the charge carrier density was extracted using the relation

$$R_0 = \frac{1}{ne} \tag{18}$$

where n is the charge carrier density and e is the charge of the electron. The charge carrier density came out to be

$$n = 1.5601752 \times 10^{24} \pm 9.3 \times 10^{18} (0.00060\%) \frac{1}{m^3} \tag{19}$$

The saturation susceptibility of nickel calculated in CGS turned out to be

$$\chi_{sat} = \frac{M_{sat}}{H_{sat}} = 18.0 \pm 1.4 (7.6\%) \tag{20}$$

This value is of the same scale as that taken from the literature [6]. Using the measurements, the coercivity of nickel in the measured axis was found to be

$$H_C = 30G$$

which is in agreement with theoretical values [4]. The susceptibility could not be measured prior to saturation due to the hysteresis loop that yields two different magnetization values for every external field, therefore χ is undefined.

9 PHE

Measurements of R_{xy} and R_{xx} were made for 38 different angles in the range $[0,\pi]$ with a constant external magnetic field $H = 3493G$. R_{xx} and R_{xy} were fitted according to equations 11 and 12 in the following manner: R_{xx} was fitted to the function

$$y = a_0 cos^2(2x) + a_1 sin^2(2x)$$

where a_0 has the theoretical value ρ_{par} and a_1 has the theoretical value ρ_{perp}. R_{xy} was then fitted to the function

$$y = b_0 sin(2x) + b_1$$

where b_0 is expected to be $\frac{\rho_{par}-\rho_{perp}}{2}$ extracted from the previous fit . The fit for R_{xx} yielded the following results (see Figure 11):

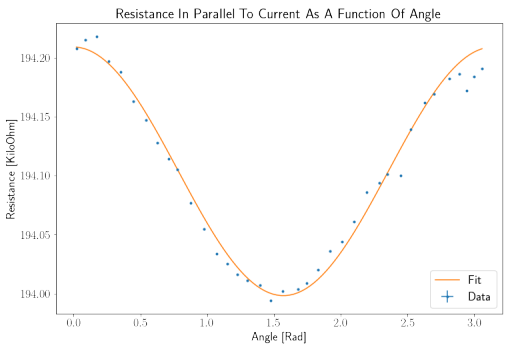

Figure 11: R_{xx} as a function of the angle between the magnetic field and current flow direction, θ

The corresponding fit parameters and statistical values are presented in Table 1.

Parameter	Value	Error (Relative Error)
$a_0[k\Omega]$	1.942×10^2	$2.42 \times 10^{-3}(0.0012\%)$
$a_1[k\Omega]$	1.940×10^2	$2.45 \times 10^{-3}(0.0013\%)$
χ^2_{red}	2.8×10^4	————
p_{value}	0.0	————

Table 1: R_{xx} fit parameters and statistical values

Using the fit parameters and according to equation 11 ρ_{par} and ρ_{perp} were both extracted

$$\rho_{par} = 1.942 \times 10^2 \pm 2.42 \times 10^{-3}(0.0012\%)[k\Omega]$$
$$\rho_{perp} = 1.940 \times 10^2 \pm 2.45 \times 10^{-3}(0.0013\%)[k\Omega] \quad (21)$$

The statistical values are out of their corresponding desired ranges, however, the fit shows that the function the data was fitted to describes the phenomena adequately with some needed tweaks as the residuals plot shows a clear trend of some high order polynomial as can be seen in Figure 12

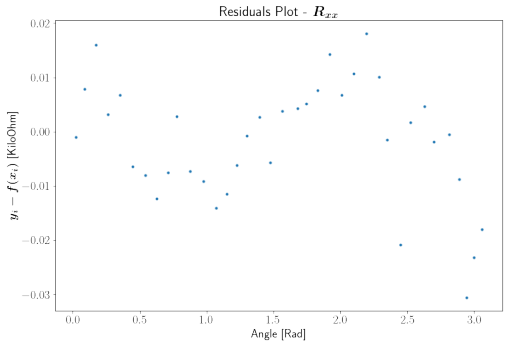

Figure 12: Residuals plot of the R_{xx} fit

Further discussion is on later sections of this report. For R_{xy} the fit yielded the following results (see Figure 13):

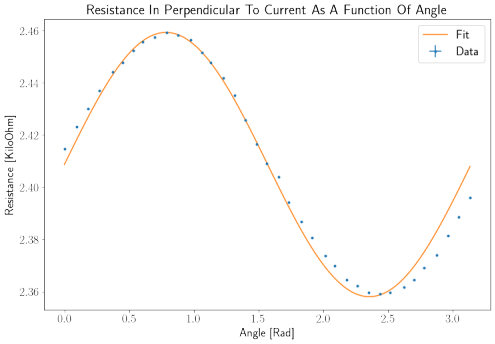

Figure 13: R_{xy} as a function of the angle between the magnetic field and current flow direction, θ

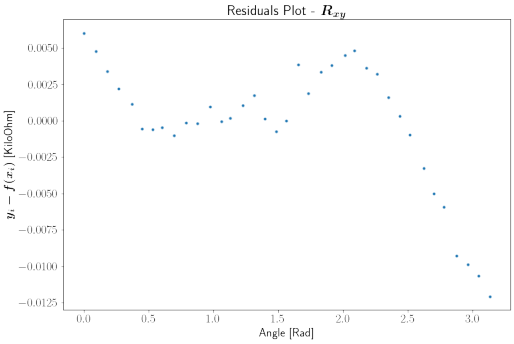

Figure 14: Residuals plot of the R_{xy} fit

The corresponding fit parameters and statistical values are presented in Table 2

Parameter	Value	Error (Relative Error)
$b_0[k\Omega]$	5.067×10^{-2}	$7.4 \times 10^{-4}(1.4\%)$
$b_1[k\Omega]$	2.40868	$6.0 \times 10^{-4}(0.025\%)$
χ^2_{red}	7.9×10^3	————
p_{value}	0.0	————

Table 2: R_{xy} fit parameters and statistical values

Similar to the previous fit, the statistical values are out of their corresponding desired ranges, yet the fit shows that the function the data was fitted to describes the phenomena adequately with some needed tweaks as the residuals plot shows a clear trend of some high order polynomial as can be seen in Figure 14

Similar problems occur for both fits. More about it in the discussion.

10 AMR

Measurements of the resistance in parallel to the current (R_{xx}) were collected while the external magnetic field was cycling from $-4300\,[Gauss]$ to $4300\,[Gauss]$. The external field was oriented in parallel, perpendicular and transversely to the current. The AMR effect is symmetric to a 180° rotation of the external field and so, the measurements were separated into the symmetric and anti-symmetric parts, as any function can be

$$f(x) = \underbrace{\frac{f(x)+f(-x)}{2}}_{\textbf{\textit{symmetric}}} + \underbrace{\frac{f(x)-f(-x)}{2}}_{\textbf{\textit{anti-symmetric}}}$$

The symmetric part includes the expected AMR effects on the resistance while the anti-symmetric part includes the temperature dependence and other effects such as AHE which occurs due to the R_{xy} contribution to the resistance, as it is not entirely parallel. To accurately find $R(H)$ and $R(-H)$ pairs (R denotes resistance, H denotes the applied field), evenly distanced measurements were interpolated on both positive and negative field values, such that both sides had the same number of measurements and at opposite fields. As there are multiple different measurements going from one end to the other in each run, the measurements were

broken up into "tracks" of single measurements from $-4300\,[Gauss]$ to $4300\,[Gauss]$, each track has its own symmetric and anti-symmetric parts.

The average resistance of the symmetric part at saturation was calculated. Points were selected depending on their distance (in standard deviations) from previous nearby points and the average. These averages represent $\rho_{Perpendicular}$ (ρ_P), $\rho_{Transverse}$ (ρ_T) and $\rho_{Parallel}$ ($\rho_\parallel$), each corresponding to its respective measurement, see Figures 15 through 17.

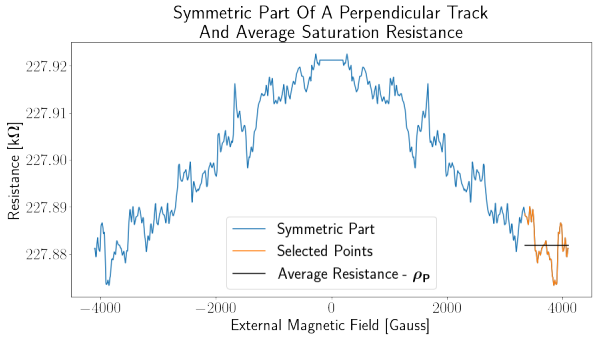

Figure 15: The extracted symmetric part of the first track for measurements with a perpendicular external field and the average resistance at saturation.

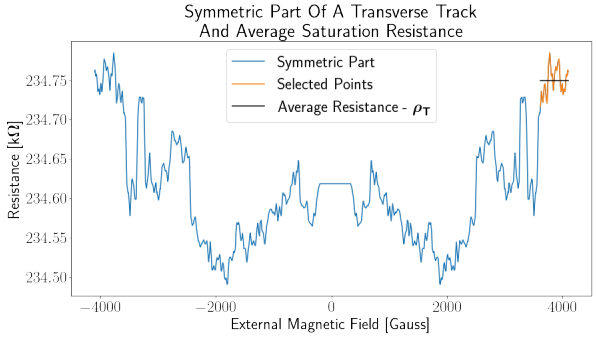

Figure 16: The extracted symmetric part of the second track for measurements with a transverse external field and the average resistance at saturation.

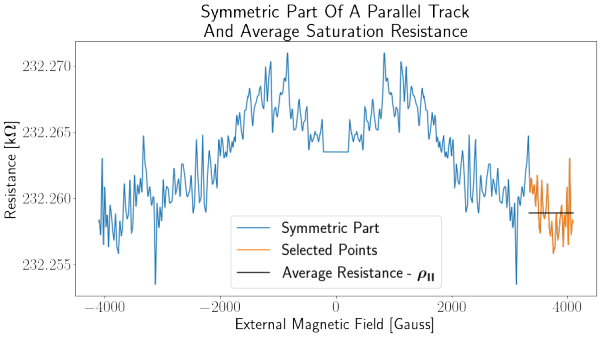

Figure 17: The extracted symmetric part of the first track for measurements with an external field parallel to the current and the average resistance at saturation.

The average resistances are presented in Table 3.

Average Resistance In Each Orientation (R.E.)
$\rho_P = 2.3225890 \times 10^2 \pm 1.1 \times 10^{-4}\,(4.7 \times 10^{-5}\%)\,[k\Omega]$
$\rho_T = 2.2788180 \times 10^2 \pm 3.1 \times 10^{-4}\,(1.36 \times 10^{-4}\%)\,[k\Omega]$
$\rho_\parallel = 2.347496 \times 10^2 \pm 1.5 \times 10^{-3}\,(6.4 \times 10^{-4}\%)\,[k\Omega]$

Table 3: Average resistances at saturation for different field orientations

The resistances are of the same order as those extracted in PHE.

The metric $\frac{\Delta\rho}{\rho} = \frac{2|\rho_P - \rho_\parallel|}{\rho_P + \rho_\parallel} = 1.1\%$ shows the scale of the AMR effect to be a small percentage of the total resistance.

More on the graphs, and resistances in the discussion.

Part IV
Discussion

Please note the change in order, AHE's discussion is last.

11 PHE

In this section of the experiment the magnetic field was applied in the same plane as the nickel plate and the an-

gle between the current flow direction and the external magnetic field was changed from the values 0 to π. Two fits were made according to equation 14 to R_{xx} and R_{xy} from which ρ_{par} and ρ_{perp} were both extracted. The relative errors on both values came out low, which can perhaps be attributed to not taking larger errors on the measurements. Regardless, the statistical values are not in their desirable ranges and a clear trend can be seen in both residuals plots. However, the behavior of the measurements matches that described by the theory, sine and cosine function do seem, for the most part to describe the phenomena. In addition to that, for $\theta = 0, \pi$ a clear maximum in the resistance be seen, matching the fact that $\rho_{par} > \rho_{perp}$ as explained in the AMR theoretical section. Similarly, for $\theta = \frac{\pi}{2}$ a clear minimum can be seen, fitting the same explanation given in the AMR section. In search for possible sources that could have altered the measurements and led to the inadequate fits a few ideas came up. First of all, the external magnetic field changes with time and the fluctuations are not random. This can also be seen in Figure 18 where the fluctuations seem to change periodically with time with a small amplitude of $50G$.

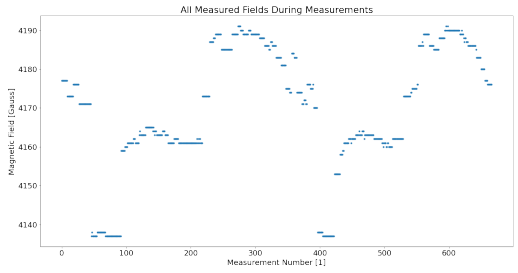

Figure 18: Field fluctuations in the magnetic field

This change might not be powerful on its own to alter measurements (as they were measured in only slightly different external magnetic fields) but can lead to slight changes. Another source of error is the hysteresis loop. The external magnetic field's direction was changed and the plate became more magnetized in that direction, however, due to hysteresis, domains magnetized in the previous direction could have remained, altering the measurements. The effects of this on our measurements may be caused by change between different directions as the applied external magnetic field saturates the magnetization in the easy axis and intermediate and nearly does so in the hard axis as was seen and explained in the AMR and AHE sections. If the magnetization is not saturated only in the hard axis (and near it) and for all other directions it is saturated, then the measurements should be mostly altered when the external magnetic field points to a hard axis. In both fits the measurements around $\theta = 0, \frac{\pi}{2}, \pi$ were problematic. The axis defined by these angles can therefore be assumed to be the hard axis. The hard axes in this case are perpendicular to each other , which fits the hard axis of a FCC lattice [9, 3]. All the effects described above contribute to the alteration of the measurements and result in the inadequate fit.

12 AMR

In this section of the experiment the magnetic field was oriented in three orthogonal directions, corresponding to the normal vector to the nickel sample (perpendicular, $\hat{z}$), the direction of the short edge (transverse, $\hat{y}$) and the direction of the long edge (parallel, $\hat{x}$) of the rectangular sample. Current was passed along $\hat{x}$, and the resistance across $\hat{x}$ was measured while the magnetic field was changed.

The resulting R-H (resistance - magnetic field) curve was separated into tracks with a single resistance for every magnetic field over the whole range. The symmetric and anti-symmetric parts of each track were extracted. From the symmetric part a rough estimate for the magnetic field required for saturation can be made and the resistance at saturation can be calculated. The resistances are of the same scale as those extracted in the previous part, PHE. The transverse and perpendicular saturation resistances are supposed to be the same (the rest of the graph is different due to magnetocrystalline energy), however that is not the case. We believe faulty connections and a mistaken measuring device are the main culprits. As can be seen in Figure 19

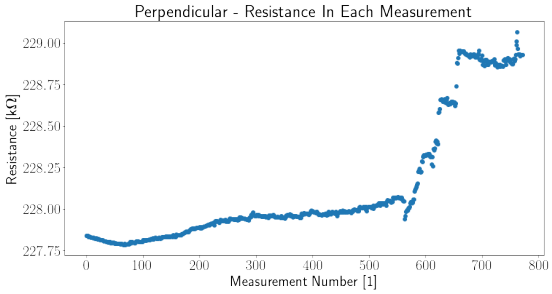

Figure 19: Measured resistance plotted against measurement number

the resistance measurements are not accurate to an order of $1\,k\Omega$, and so, the difference is of the magnitude of the system's resolution, i.e. $1\,k\Omega$. The change in the resistances of the transverse and the parallel fields are inconsistent with the theory. The transverse field saturates at a higher resistance than it started at and is not monotonic. In addition, the parallel field saturates at a lower, rather than higher resistance and monotonically decreases as opposed to increasing. Both graphs contradict Figure 7. There are two possible explanations for these results. The first, that a mix-up between the two measurements was made, however, that is highly unlikely as the measurements were done in separate excel files, meaning, the mistake had to happen twice. The second explanation is that the connections were faulty, or that the wrong connections were made.
By looking at the symmetric parts and estimating at which field strength the average resistance no longer changes, the field required to saturate the magnetization along that axis is found. Our estimates are $H^P_{sat} \approx 3000\,[Gauss]$, $H^T_{sat} \approx 2500\,[Gauss]$ and $H^{\parallel}_{sat} \approx 2000\,[Gauss]$, these suggest that the hard axis of the fcc crystal is mostly along $\hat{z}$, and the easy axis is mostly along $\hat{x}$. This finding is opposed to the result in the AHE which suggests that the easy axis is mostly along $\hat{z}$, this may also corroborate the hypothesis that the measurements of the parallel and transverse parts were mixed up or that the connections were faulty.

13 AHE

The extracted values from the anomalous Hall effect are of the same scale as values from the literature and as can be seen in Figure 10 a clear hysteresis loop can be seen and both the normal and anomalous Hall effects can be observed. The saturation magnetization may have been smaller or bigger than its final value as the way it was estimated offers freedom and allows to perform linear fits with data from different regions, yielding different intersection points and thus different saturation magnetizations. In this part of the experiment, the external magnetic field was directed perpendicular to the plane of the nickel sample, along $\hat{z}$, and the coercivity and width of the hysteresis loop align with values corresponding with those belonging to the easy axis of nickel, which suggests that $\hat{z}$ is the easy axis of the material. As was mentioned in the AMR section, there is a difference between the results from AMR and the results from this experimental part, which can be attributed to faulty connections of the experimental system as the results from AMR prove significantly different from the expected theoretical behavior. Regardless of the inability to extract convincing information about the sample from the AMR section, both PHE and AHE support the claim that the easy axis lies in the z direction.

References

[1] Gerd Bergman. *Physics Today*, 32, 1979.

[2] B.Legendre and M.Sghaier. *Springer*, 2011.

[3] Robert C.O'Handley. *Modern Magnetic Materials Principles and Applications*. JOHN WBkEY and SONS, INC, 2000.

[4] M.S Miller, F.E Stageberg, Y.M Chow, K.Rook, and L.A. Heuer. *J.Appl*, 75, 1994.

[5] J.J. Sakurai and Jim Napolitano. *Modern Quantum Mechanics Second Edition*. Pearson, 2011.

[6] John F. Schenck. *Medical Physics*, 23, 1996.

[7] Steven H. Simon. *The Oxford Solid State Basics*. OXFORD University Press, 2013.

[8] Nicola A. Spaldin. *Magneitc Materials Fundamentals and Applications*. Cambridge University Press, 2011.

[9] G.P. Thomson. *Nature*, 123, 1929.